PHYSICAL REVIEW B **73**, 184110 (2006)

Fragile phase stability in $(1-x)Pb(Mg_{1/3}Nb_{2/3}O_3)$-$xPbTiO_3$ crystals: A comparison of [001] and [110] field-cooled phase diagrams

Hu Cao, Jiefang Li, and D. Viehland
Department of Materials Science and Engineering, Virginia Tech, Blacksburg, Virginia 24061, USA

Guangyong Xu
Condensed Matter Physics and Materials Science Department, Brookhaven National Laboratory, Upton, New York 11973, USA

(Received 3 February 2006; revised manuscript received 28 March 2006; published 9 May 2006)

Phase diagrams of [001] and [110] field-cooled (FC) $(1-x)Pb(Mg_{1/3}Nb_{2/3}O_3)$-$xPbTiO_3$ or PMN-xPT $(0.15 \leqslant x \leqslant 0.38)$ crystals have been constructed, based on high-resolution x-ray diffraction data. Comparisons reveal several interesting findings. First, a region of abnormal thermal expansion $(c \neq a)$ above the dielectric maximum was found, whose stability range extended to higher temperatures on application of electric field (E). Second, the rhombohedral (R) phase of the zero-field-cooled (ZFC) state was replaced by monoclinic M_A in the [001] FC diagram, but with monoclinic M_B in the [110] FC. Third, the monoclinic M_C phase in the ZFC and [001] FC diagram was replaced by an orthorhombic (O) phase in the [110] FC diagram. Finally, in the [001] FC diagram, the phase boundary between tetragonal (T) and M_A phases was extended to lower PT content $(x=0.25)$; whereas in the [110] FC diagram, this extended region was entirely replaced by the O phase. These results clearly demonstrate that the phase stability of PMN-xPT crystals is quite fragile—depending not only on modest changes in E, but also on the direction along which E is applied.

DOI: 10.1103/PhysRevB.73.184110 PACS number(s): 61.10.Nz, 77.84.Dy

I. INTRODUCTION

Solid solutions of $(1-x)Pb(Mg_{1/3}Nb_{2/3}O_3)$-$xPbTiO_3$ (PMN-xPT) and $(1-x)Pb(Zn_{1/3}Nb_{2/3}O_3)$-$xPbTiO_3$ (PZN-xPT), have attracted much interests as high-performance piezoelectric actuator and transducer materials.[1] For example, (001)-oriented PMN-0.33PT crystals, which lies inside a morphotropic phase boundary (MPB), have the highest piezoelectric ($d_{33} \sim 2500$ pC/N) and electromechanical coupling ($k_{33} \sim 94\%$) coefficients.[2] Historically, the high electromechanical properties of $Pb(Zr_x, Ti_{1-x})O_3$ (PZT) ceramics were attributed to the nearly vertical MPB between rhombohedral (R) and tetragonal (T) ferroelectric phases,[3] resulting in phase coexistence. Park and Shrout conjectured that the exceptional electromechanical properties of oriented PMN-xPT and PZN-xPT crystals were rather due to a $R \rightarrow T$ phase transition induced by an applied electric field (E).[1,4]

More recently, various intermediate monoclinic phases that structurally "bridge" the R and T ones across the boundary have been reported in PZT ceramics,[5–7] and subsequently in PZN-xPT (Refs. 8–12) and PMN-xPT (Refs. 12–17) crystals—i.e., the MPB is not so vertical and sharp. Monoclinicity may be important in that it allows the polarization vector to be unconstrained within a plane,[18] rather than constricted to a particular crystallographic axis as for the higher-symmetry R, T, or orthorhombic (O) phases, as shown in Fig. 1(a). Two types of monoclinic distortions M_A and M_C have been reported, which correspond to space groups Cm and Pm, respectively. The M_A unit cell has a unique b_m axis along the [110] direction, and is doubled and rotated 45° about the c axis, with respect to the pseudocubic cell; whereas, the M_C unit cell is primitive having a unique b_m axis that is oriented along the pseudocubic [010]. Recently, a monoclinic M_B phase has been reported:[17] although both the M_A and M_B phases belong to the Cm space group, the difference lies in the magnitudes of the components of the polarization[19] corresponding to the pseudocubic cell: for the M_A phase, $P_x = P_y < P_z$, whereas for the M_B phase, $P_x = P_y > P_z$. In addition, an O ferroelectric phase has been reported to be induced by E in (001) PZN-0.08PT crystals,[8] and by a field applied along (110) in PMN-0.30PT.[17] This O phase is the limiting case of a M_C phase, which can be considered as $a_m = c_m$, similar to that of $BaTiO_3$.[20]

Recent diffraction experiments under electric field (E) have shown that the phase stability of PMN-xPT and PZN-xPT is dependent upon the electrical history of the crystal. Neutron studies of PZN-0.08PT crystals with $E \| [001]$,[11] have shown a $C \rightarrow T \rightarrow M_C$ phase sequence in the field-cooled (FC) condition, but a $R \rightarrow M_A \rightarrow M_C \rightarrow T$ one with increasing E beginning from the zero-field-cooled (ZFC) state. Similarly, neutron and x-ray diffraction investigations[15] of PMN-0.30PT have established a $C \rightarrow T \rightarrow M_C \rightarrow M_A$ sequence in the $E \| [001]$ FC condition, but a $R \rightarrow M_A \rightarrow M_C \rightarrow T$ one with increasing E beginning from the ZFC state. Dielectric property studies of PMN-0.33PT crystals[21] with $E \| [110]$ have reported a mestastable O phase, bridging T and R phases, over a narrow temperature range in the FC condition. Polarized light microscopy indicated that this O phase was a single-domain one. A recent structural study[17] of PMN-0.30PT with $E \| [110]$ has unambiguously shown a $C \rightarrow T \rightarrow O \rightarrow M_B$ sequence in the FC condition, but a $R \rightarrow M_B \rightarrow O$ one with increasing E beginning from the ZFC sample at 300 K. These prior studies clearly evidence that the phase stability of PMN-xPT crystals is altered by the electrical history and by the crystallographic direction along which E is applied. However, a systematic investigation of the phase stability has not yet been performed over a wide compositional range of x. Thus, understanding of how the

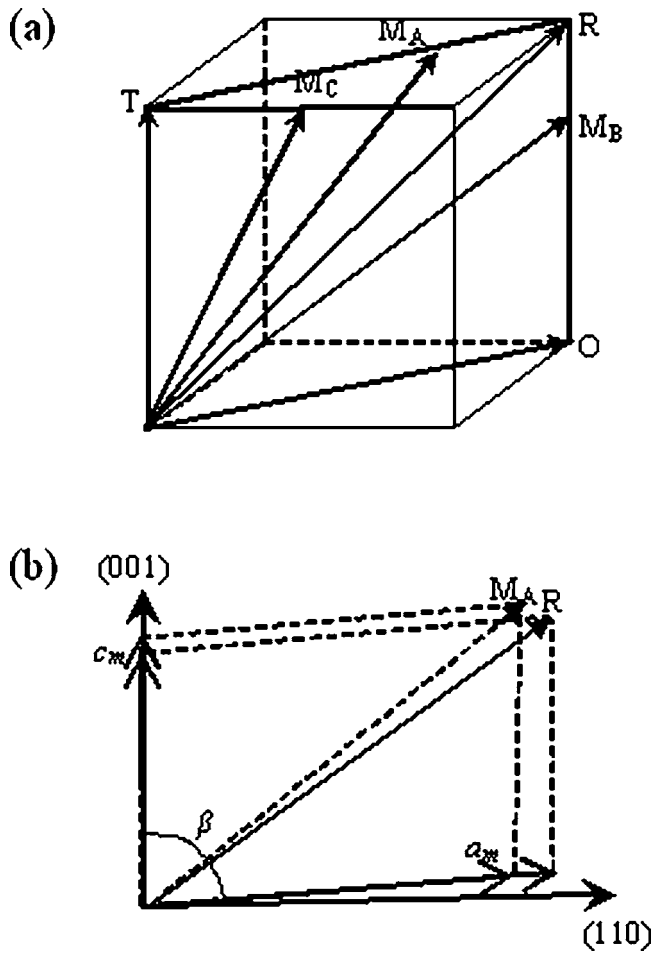

FIG. 1. (a) Rotation of polarization vectors in monoclinic perovskite unit cells. The thick lines represent the paths followed by the end of the polarization vector in the M_A phase where the polarization rotates in a plane between rhombohedral (R) and tetragonal (T), in the M_B phase where the polarization rotates between R and orthorhombic (O) phases, and in the M_C phase where the polarization rotates between O and T phases. The M_A, M_B, and M_C notation is adopted following Vanderbilt and Cohen (Ref. 18). (b) Polarization vectors of the rhombohedral (R) and monoclinic M_A (Cm) phases, represented with the same monoclinic angle β in the HHL zone of reciprocal space. The R unit cell can be expressed in terms of a monoclinic one by $a_m=2a_r\cos(\alpha/2)$, $b_m=2a_r\sin(\alpha/2)$, $a_m=a_r$, $\cos(\beta)=[1-2\sin^2(\alpha/2)]/\cos(\alpha/2)$, where a_r and α are the $R3m$ cell parameters.

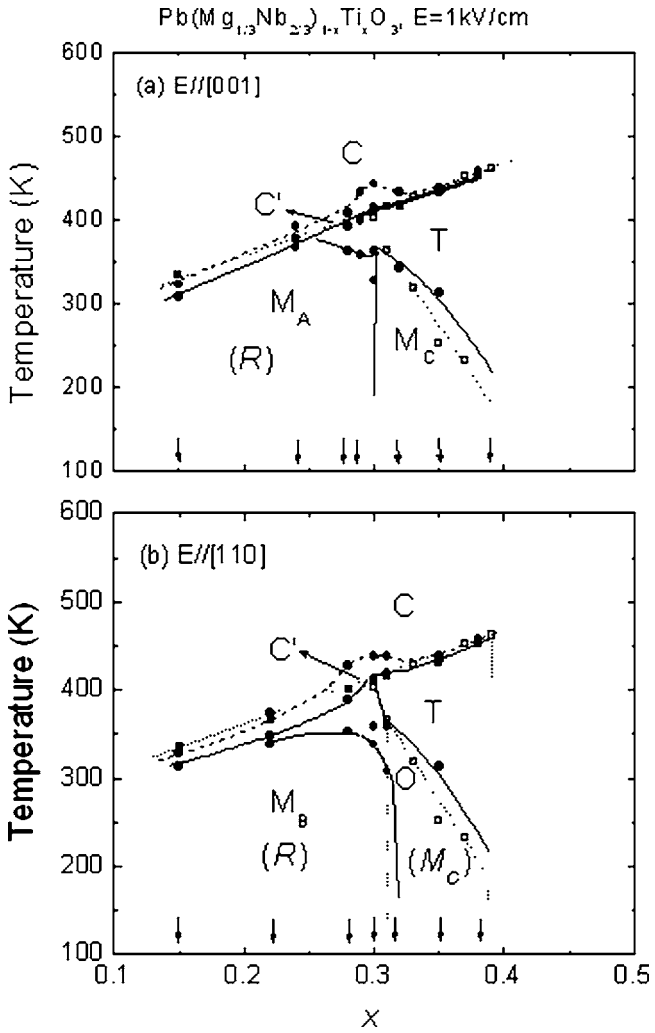

FIG. 2. Modified phase diagrams of (a) [001] and (b) [110] electric-field-cooled PMN-xPT crystals. The dotted lines and open square signs were based on prior studies by Noheda *et al.* (Ref. 14). The bracketed italic R and M_C represent the rhombohedral and monoclinic phases of the zero-field-cooled condition. The solid squares represent the temperature of the dielectric maximum (T_M). The solid circles represent the temperature of the phase transition in the FC condition. The C' phase below the upper dashed curve was determined by a region of abnormal thermal expansion. Solid curves drawn through these data point are only to guide the eyes.

phase diagram is altered by the direction along which E is applied is limited.

Here, we report a high-resolution x-ray diffraction study of [001] and [110] FC PMN-xPT crystals of numerous compositions, both near and away from the MPB. Our findings are summarized in Fig. 2. The dotted lines and open squares are based on prior studies by Noheda *et al.*[14] R and M_C represent the rhomboheral and monoclinic phases of the zero-field-cooled condition. The solid squares represent the temperature of the dielectric maximum (T_M) in the ZFC condition. The solid circles represent the temperature of the phase transition in the FC condition determined by the x-ray diffraction in this study. The C' phase below the upper dashed curve was determined by a region of abnormal thermal expansion. Solid curves drawn through these data point are only to guide the eyes. We have determined how the stability regions of the various intermediate phases are altered by E and the direction along which it is applied. The results demonstrate that the phase diagram of PMN-xPT crystals is quite fragile—depending not only on modest changes in E, but also on the direction along which E is applied.

II. EXPERIMENTAL PROCEDURE

Single crystals of PMN-xPT (x=0.38, 0.35, 0.32, 0.30, 0.28, 0.27, 0.24, 0.15) with dimensions of 3×3

$\times 3$ mm^3 were obtained from HC Materials (Urbana, IL), and were grown by a top-seeded modified Bridgman method. Two kinds of cubes were cut along the pseudocubic (001)/(100)/(010) and (110)/(1$\bar{1}$1)/($\bar{1}$12) planes, and were polished to 0.25 μm. Gold electrodes were deposited by sputtering. Temperature-dependent dielectric constant measurements were performed using a multifrequency LCR meter (HP 4284A) under various E.

The x-ray diffraction studies were performed using a Philips MPD high-resolution system equipped with a two-bounce hybrid monochromator, an open three-circle Eulerian cradle, and a domed hot stage. A Ge (220)-cut crystal was used as an analyzer, which had an angular resolution of 0.0068°. The x-ray wavelength was that of Cu $K\alpha$=1.5406 Å, and the x-ray generator was operated at 45 kV and 40 mA. The penetration depth in the samples was on the order of 10 μm. For (001) field cooled PMN-xPT crystals, we performed mesh scans around the (002) and (200) Bragg reflections in the $(H,0,L)$ zone, defined by the [001] and [100] vectors; and about the (220) reflection in the scattering (H,H,L) zone, defined by the [110] and [001] vectors. For (110) field-cooled PMN-xPT, the domain structure is more complicated: we performed mesh scans around the (002) reflection in the (H,H,L) zone, defined by the [001] and [110] vectors; the (220) and (2$\bar{2}$0) reflections in the scattering zone defined by the [110] and [1$\bar{1}$0] vectors; and the (200) in the $(H0L)$ zone, defined by the [100] and [001] vectors. Each measurement cycle was begun by heating up to 550 K to depole the crystal, and measurements were subsequently taken on cooling. In this study we fixed the reciprocal lattice unit $a^*=2\pi/a$ =1.560 Å^{-1}. All mesh scans of PMN-xPT shown in this study were plotted in reference to this reciprocal unit.

III. RESULTS

A. [001] electric-field-cooled PMN-xPT

Figure 3 shows the temperature evolution of the lattice parameters for [001] FC PMN-xPT crystals whose composition is to the left of the MPB: x=0.15, 0.24, 0.27, and 0.28. Previously, we have reported these data for compositions near and to the right of the MPB; x=0.30,[15] 0.32,[16] and 0.35.[22]

For PMN-0.15PT and PMN-0.24PT, only a single phase transition was observed on cooling under a field of E =0.5 kV/cm. However, there was an important difference between the temperature evolutions of the lattice parameters for these two compositions. Specifically for x=0.15, we observed the lattice parameter $a_m/\sqrt{2}$ to be notably larger than c_m; whereas for x=0.24, we found $a_m/\sqrt{2}<c_m$ where on cooling the value of $a_m/\sqrt{2}$ approached that of c_m. Diffraction results then confirmed that these two crystals had identical domain configurations in their low-temperature phases, belonging to the Cm space group. Using the values of $a_m/\sqrt{2}c_m$ and β, we conclude that both PMN-0.15PT and PMN-0.24PT have the monoclinic M_A structure (please see the Appendix for details).

For PMN-0.27PT and PMN-0.28PT, two phase transitions were observed on electric-field cooling with the sequence

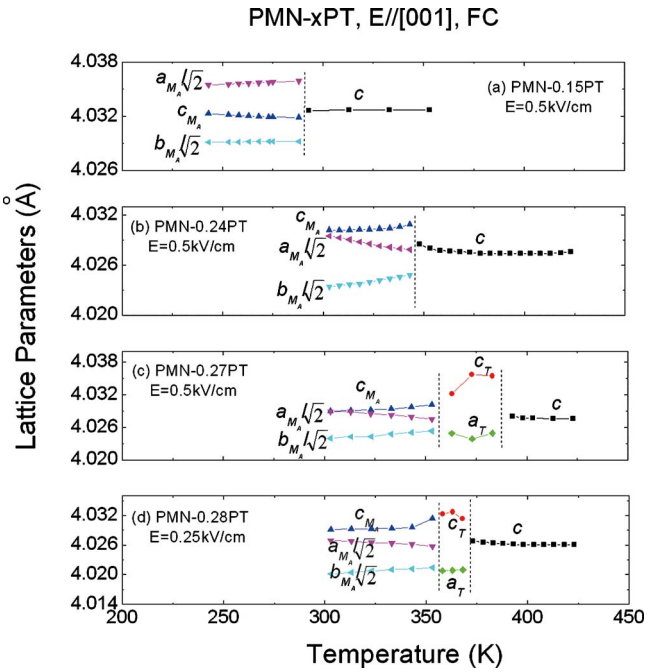

FIG. 3. (Color online) Lattice parameters as a function of temperature for [001] field-cooled PMN-xPT crystals: (a) PMN-0.15PT, E=0.5 kV/cm; (b) PMN-0.24PT, E=0.5 kV/cm; (c) PMN-0.27PT, E=0.5 kV/cm; and (d) PMN-0.28PT under E=0.25 kV/cm.

$C\rightarrow T\rightarrow M_A$. In addition, we observed for both crystals that the lattice parameter $a_m/\sqrt{2}$ increased with decreasing temperature, approaching c_m. The principal difference between the results with increasing PT content in this range was that the field required to stabilize the T phase on cooling was reduced with increasing x: E=0.50 kV/cm for x=0.27, but E=0.25 kV/cm for x=0.28. For $x\geqslant 0.3$, M_C is the dominant monoclinic phase, as the composition enters the region of the MPB: the transformational sequence for x=0.30 is $C\rightarrow T\rightarrow M_C\rightarrow M^A$,[15] whereas that for x=0.32 and 0.35 is $C\rightarrow T\rightarrow M_C$.[16,22] For $x\geqslant 0.38$, the T phase was stable down to 243 K, with a transformational sequence of simply $C\rightarrow T$.

Next, we measured changes in mesh scans with increasing x in the [001] FC condition. Figure 4 shows a partial summary of the many measurements made at lower temperatures for various PMN-xPT compositions across the phase diagram. The mesh scans of the low-temperature phase with $0.15\leqslant x\leqslant 0.30$ were consistent with the known signatures for the M_A phase;[10,15] whereas those with $0.32\leqslant x\leqslant 0.35$ were consistent with the M_C phase.[8,11,15] Mesh scans at various temperatures confirmed signatures of the phase transformational sequences noted above for the various compositions.

Our findings for [001] PMN-xPT are summarized in the phase diagram given in Fig. 2(a), above. The [001] FC transformational sequence was $C\rightarrow M_A$ for $x<0.25$, $C\rightarrow T\rightarrow M_A$ for $0.25\leqslant x\leqslant 0.3$; $C\rightarrow T\rightarrow M_C$ for $0.3\leqslant x\leqslant 0.35$; and $C\rightarrow T$ for $x>0.35$. Based on lattice parameter studies, we found that the intermediate T phase extends to x=0.25 in the FC condition, rather than x=0.3 as for the ZFC condition. Previous reports of dielectric relaxation[23] in the temperature range of this extended T phase indicate that microdomains of

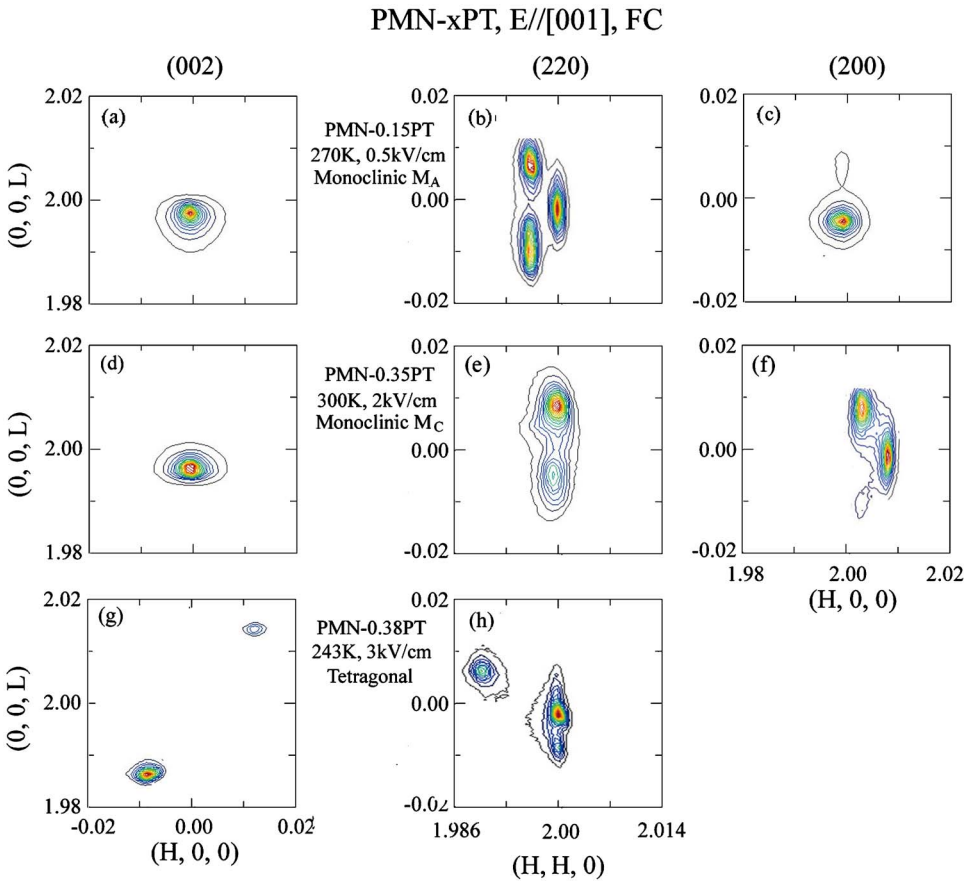

FIG. 4. (Color online) Mesh scans taken about the pseudocubic (002), (220), and (200) reflections for [001] field-cooled PMN-xPT crystals: (a) PMN-0.15PT, $E=0.5$ kV/cm at 270 K; (b) PMN-0.35PT, $E=2$ kV/cm at 300 K; and (c) PMN-0.38PT, $E=3$ kV/cm at 243 K.

tetragonal symmetry may be stabilized by application of $E\|[001]$ over a narrow phase region, on cooling from the cubic to the M_A phase. This possibility is further substantiated by the observation that the $C\rightarrow T$ boundary as determined by structural data ($c>a$) was found to shift to higher temperatures with increasing field for $E<3$ kV/cm, whereas the $C')\rightarrow T$ boundary determined by the dielectric maximum was independent of E: these results will be discussed in more detail in Sec. IV.

B. (110) electric-field-cooled PMN-xPT

Figure 5 shows the temperature evolution of the lattice parameter for [110] FC PMN-xPT with $x=0.15$, 0.22, and 0.28. Results for PMN-0.30PT (Ref. 17) and PMN-0.35P (Ref. 22) have recently been reported, and can be found in the corresponding references.

For $0.15\leqslant x\leqslant 0.20$, a single phase transition was observed on cooling under $E=0.5$ kV/cm. Structural analysis confirmed that the low-temperature phase had a M_B lattice symmetry, with $a_m/\sqrt{2}>c_m$; and thus, the transformational sequence on cooling is $C\rightarrow M_B$. Temperature-dependent lattice parameter studies revealed that the difference between $a_m/\sqrt{2}$ and c_m gradually increased with decreasing temperature in the M_B phase field, contrary to the observed increase in the M_A phase field from the [001] FC measurements. For $0.22<x<0.28$, two phase transitions were observed on field cooling. Structural analysis revealed the transformational sequence to be $C\rightarrow O\rightarrow M_B$: no intermediate T phase was found to extend over to lower PT contents under E; rather a single-domain O phase was found in its place. For $x=0.22$, coexistence of O and M_B phases was observed under $E\leqslant 1.0$ kV/cm, but with increasing field to $E=2$ kV/cm such

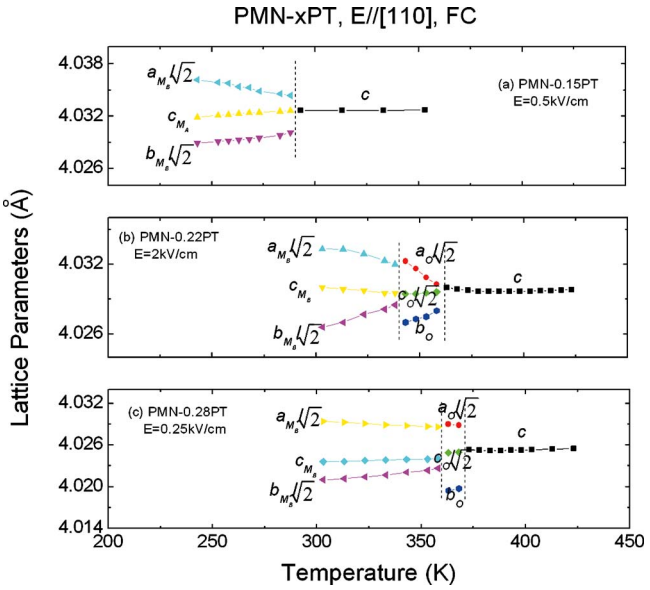

FIG. 5. (Color online) Lattice parameters as a function of temperature for [110] field-cooled PMN-xPT crystals: (a) PMN-0.15PT, $E=0.5$ kV/cm; (b) PMN-0.22PT, $E=2$ kV/cm; and (c) PMN-0.28PT, $E=0.25$ kV/cm.

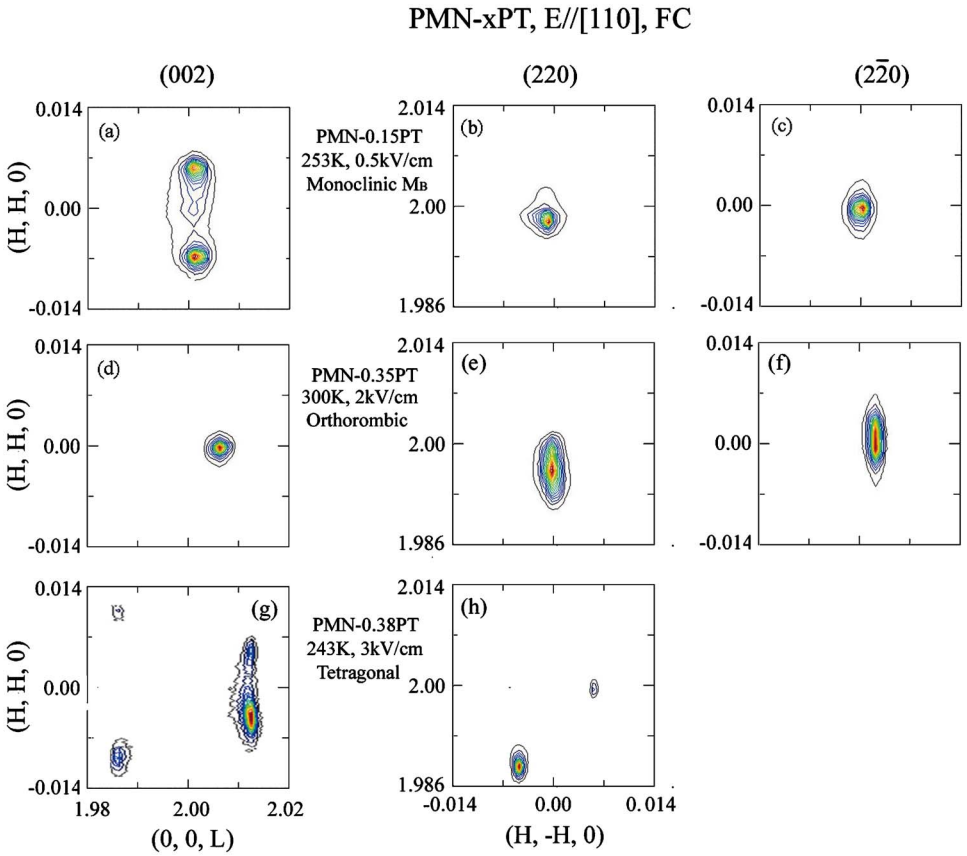

FIG. 6. (Color online) Mesh scans taken about the pseudocubic (002), (220), and (200) reflections for [110] field-cooled PMN-xPT crystals: (a) PMN-0.15PT, $E=0.5$ kV/cm at 253 K; (b) PMN-0.35PT, $E=2$ kV/cm at 300 K; and (c) PMN-0.38PT, $E=3$ kV/cm at 243 K.

coexistence was not found. With increasing x between 0.22 and 0.28, the field required to stabilize the O phase on cooling was found to be decreased. For $0.30 \leqslant x \leqslant 0.35$, an intermediate T phase was found, similar to that in the ZFC condition. Over a narrow compositional range near $x \approx 0.30$, the transformational sequence was found to be $C \rightarrow T \rightarrow O \rightarrow M_B$; whereas for $x=0.32$ and 0.35, we found the sequence to be $C \rightarrow T \rightarrow O$. For $x > 0.32$, the T phase was found to become increasingly dominant with increasing x; until for $x=0.38$, the sequence was simply $C \rightarrow T$.

Next, we also measured changes in mesh scans of PMN-xPT ($x=0.15, 0.35, 0.38$) at low temperatures in the [110] FC condition, as shown in Fig. 6. Results from one crystal are shown here, which reveal the signatures of both the M_B and O phases. We illustrate the signatures of the M_B phase using results for $x=0.15$ as shown in Figs. 6(a), 6(b), and 6(c). At 253 K, the (220) reflection reveals a single peak, indicating that $E \| [110]$ fixes the [110] crystallographic direction of the crystal: two peaks about the (002) reflection were found, which were split along the transverse direction L; and the (2$\bar{2}$0) reflection and (200) reflection (not shown) also revealed a single peak. The combination of these mesh scans provides the signatures of M_B—two polarization vectors constrained to the (110) plane that lie close to [110]. A similar M_B lattice structure was found for $x=0.22$, 0.28, and 0.30 at low temperatures.[17] The signatures of the O phase are illustrated in Figs. 6(d)–6(f) for $x=0.35$, taken at 300 K in the FC condition at $E=2$ kV/cm. All mesh scans taken about the (220), (220), (002), and (200) reflections revealed a single peak—demonstrating that a single-domain O phase has been induced. For $x=0.38$, the domain configurations as shown in Figs. 6(g) and 6(h) show that the T phase remains stable on cooling to 243 K at $E=3$ kV/cm.

Our findings for [110] PMN-xPT are summarized in the phase diagram given in Fig. 2(b), above. The [110] FC transformational sequence was $C \rightarrow M_B$ for $x \leqslant 0.20$, $C \rightarrow O \rightarrow M_B$ for $0.22 \leqslant x < 0.3$; $C \rightarrow T \rightarrow O \rightarrow M_B$ for $x \approx 0.30$; $C \rightarrow T \rightarrow O$ for $0.31 < x \leqslant 0.36$; and $C \rightarrow T$ for $x > 0.37$. Based on lattice parameter studies, we found that the intermediate T phase extends to $x=0.25$ in the FC condition, rather than $x=0.3$ as for the ZFC condition. Compared to the [001] FC phase diagram, in the [110] phase diagram, an extended O phase replaces the T and M_C phases, and a M_B phase replaces the M_A phase.

IV. DISCUSSION

Comparison of the [001] and [110] FC phase diagrams of PMN-xPT in Fig. 2 reveals several interesting findings, including (i) that the R phase of the ZFC state is replaced by M_A in the [001] FC diagram, but with M_B in the [110] FC diagram; (ii) that there is a region (C') of abnormal thermal expansion ($c \neq a$) above the dielectric maximum, whose stability range is extended to higher temperatures by application of E; (iii) that the M_C phase in the [001] FC diagram is replaced by the O phase in the [110] FC diagram; and (iv) that the stability of the T phase is extended to $x=0.25$ in the [001] FC diagram, whereas this extended T-phase region is entirely replaced by the O phase in the [110] FC diagram.

It is important to note that differences between the [001] and [110] phase diagrams was caused by moderate electric

TABLE I. Calculated value of $a_m/\sqrt{2}$ and $\sqrt{2}\cos(\alpha^*/2)$ for low-temperature phases in [001] and [110] electric-field-cooled PMN-xPT crystals. β, $a_m/\sqrt{2}$, and c_m were directly derived from the experiments and the imaginary rhombohedral angle α^* was determined according to $\cos(\beta)=[1-2\sin^2(\alpha^*/2)]/\cos(\alpha^*/2)$.

x	T (K)	E (kV/cm)	$a_m/\sqrt{2}$ (Å)	c_m (Å)	β (deg)	α^* (deg)	$a_m/(\sqrt{2}c_m)$	$\sqrt{2}\cos(\alpha^*/2)$	$a_m/2c_m\cos(\alpha^*/2)$	S
					$E//[001]$					
0.30	300	1.0	4.0245	4.0242	89.950	89.965	1.0001	1.0003	0.9998	M_A
0.28	353	0.25	4.0258	4.0314	89.895	89.965	0.9986	1.0007	0.9979	M_A
0.27	300	0.35	4.0299	4.0280	89.850	89.894	1.0005	1.0010	0.9995	M_A
0.24	300	0.5	4.0295	4.0302	89.870	89.908	0.9998	1.0008	0.9990	M_A
0.15	270	0.5	4.0348	4.0319	89.885	89.917	1.0007	1.0008	0.9999	M_A
					$E//[110]$					
0.30	300	1.0	4.0280	4.0200	89.850	89.894	1.0020	1.0010	1.0009	M_B
0.28	353	0.25	4.0287	4.0240	89.900	89.929	1.0012	1.0006	1.0006	M_B
0.22	333	2.0	4.0322	4.0295	89.920	89.945	1.0007	1.0005	1.0002	M_B
0.15	243	0.5	4.0368	4.0319	89.853	89.897	1.0012	1.0009	1.0003	M_B

fields of $0.25 \leqslant E \leqslant 0.5$ kV/cm—clearly demonstrating that the phase stability of PMN-xPT crystals is quite fragile, or, simply put, many phases are apparently very close to being energetically degenerate. This phase fragility brings into question conventional wisdom concerning the thermodynamics of classical phase diagrams—indicating the important role of underlying structural heterogeneity.

A. The M_A and M_B phases

The M_A and M_B phases belong to the same group Cm; accordingly, their mesh scans exhibit identical contour features. However, we can distinguish M_A from M_B using β and the ratio $a_m/\sqrt{2}c_m$ (see the Appendix for details). Table I shows calculated values of $a_m/\sqrt{2}c_m$ and $\sqrt{2}\cos(\alpha^*/2)$ for [001] and [110] FC PMN-xPT. Using this table, we can identify the polarization rotation pathway. For [001] FC PMN-0.15PT, it was found that $a_m/\sqrt{2} > c_m$ over the entire phase field of the low-temperature phase. Thus, we can conclude that the polarization is constrained to the $R \rightarrow T$ path of the M_A phase, and it is not possible that it would follow the $R \rightarrow O$ one of M_B. However, for [110] FC PMN-xPT with $0.15 < x < 0.3$, it was found that $a_m/\sqrt{2}c_m > \sqrt{2}\cos(\alpha^*/2)$ over the entire phase field of the low-temperature phase, demonstrating that polarization rotation occurs toward [110] away from [111], following the path $R \rightarrow O$ of the M_B phase.

We note several other important points. For $x=0.15$, the difference between $a_m/\sqrt{2}c_m$ and $\sqrt{2}\cos(\alpha^*/2)$ is very small, demonstrating that the polarization vector lies quite close to [111]. Second, for [001] FC PMN-xPT with $0.24 \leqslant x \leqslant 0.27$, we observed that the value of $a_m/\sqrt{2}$ approaches that of c_m with decreasing temperature. This demonstrates that the polarization of the M_A phase gradually rotates back on cooling toward [111] and away from the [001].

B. The C' phase

Both the [001] and [110] phase diagrams of PMN-xPT exhibited a region of abnormal thermal expansion, designated as C'. In this region the lattice parameter c derived from the (002) reflection was found not to be equal to that of a derived from the (200) reflection. In addition, it was observed that the stability of the C' phase was extended to higher temperatures following application of E. As an example, Fig. 7 shows the temperature dependence of the lattice parameters derived from the (002) reflection for PMN-0.28PT in the FC state at various fields for (a) $E \| [001]$, and (b) $E \| [110]$. Both figures show that the region of $c/a > 1$ extends to higher temperatures with increasing E. Please note for $E=2$ kV/cm that the lattice parameters changed continuously with decreasing temperature, rather than exhibiting an abrupt anomaly as for $E=0.25$ kV/cm.

We are careful to distinguish the boundary C' from that of the true cubic C: C was determined from the Curie temperature (T_C) of the dielectric maximum, whereas C' from the temperature at which c/a first deviated from 1. Thus, in the phase field C', we have tetragonal splitting that occurs above the temperature of the dielectric maximum. This is unconventional with respect to normal phase transitions, where symmetry breaking occurs at or below T_C, but never above. Rather, it has some similarities to relaxor ferroelectric behavior in PMN, where local polarizations are known to exist above the dielectric maximum. Accordingly, we attribute this anomalous phase field C' to polar nanoregions (PNRs). However, there are important differences between the phase field C' and a relaxor state. Relaxors are well known to have a pseudocubic structure. Averaging over PNRs that are randomly distributed among all possible domain variants on a nanometer length scale yields a cubic structure on average. However, in the phase field C', under $E \| [001]$ or $E \| [110]$, the PNRs will be partially aligned under the direction of the applied E. Thus, the local structural asymmetric distortions of the PNRs will not be averaged to cubic; rather an ensemble of PNRs will exhibit a net distortion. Accordingly, a symmetry breaking above T_C may be observed, which gradually changes with E and temperature as the topological arrangement of PNRs is altered.

Here, we consider the structural evolution from the cubic to the ferroelectric state to occur in three steps. First, near T_B (Burns temperature), clusters of short-range polar order (i.e.,

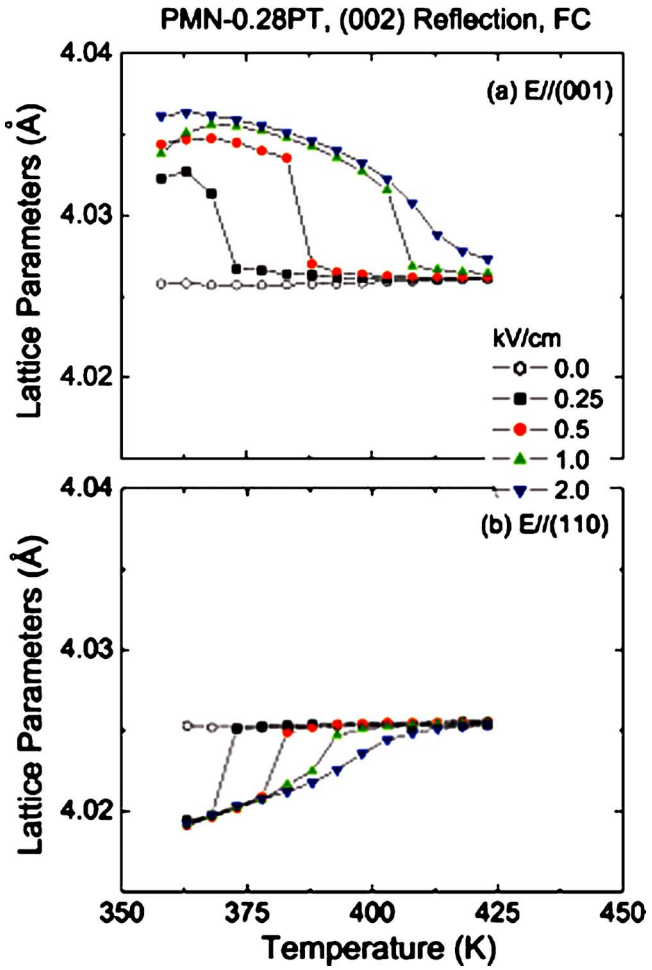

FIG. 7. (Color online) Lattice parameter as a function of temperature derived from the (002) reflection of PMN-0.28PT under different electric field levels applied along (a) $E\|[001]$, and (b) $E\|[110]$.

PNRs) develop and gradually increase in number on cooling. Second, with decreasing temperature, the ensemble of PNRs becomes percolating, resulting in the development of microdomains. However, since these microdomains are on a scale much smaller than the x-ray coherence length, only a slight broadening of the Bragg reflections is observed. This evolution is believed to be continuous and the dielectric behavior correspondingly varies smoothly on cooling. Third, below a temperature that we designate as T_M, a thermally activated formation of critical ferroelectric nuclei occurs from the microdomain state—below which point, a long-range-ordered ferroelectric phase is stable. Application of a field assists in aligning the PNR along the direction that E is applied, resulting in PNR growth and an increase in its numbers, giving rise to the abnormal thermal expansion above T_C that defines the C' phase field. Higher fields favor PNR growth at higher temperature; and correspondingly, the $C' \rightarrow C$ phase boundary is shifted to higher temperature with increasing E.

It is worth noting that the stability range of the C' phase field was extremely narrow when the stable low-temperature phase was tetragonal in both the [001] and [110] phase diagrams. The C' phase field widens significantly with increasing E only in the region where the transformational sequence was altered by changing the direction along which E was applied. The most pronounced changes were found for $x \approx 0.30$ where the sequence was $C \rightarrow C' \rightarrow T \rightarrow M_C \rightarrow M_A$ for $E\|[001]$, but $C \rightarrow C' \rightarrow T \rightarrow O \rightarrow M_B$ for $E\|[110]$. These observations suggest that the fragileness of the phase stability might be related to the structural inhomogeneity originating from the PNR state. Recent experiments on PZN-xPT relaxor systems suggest that an external electric field along the [111] direction actually enhances PNR with polarizations perpendicular to, instead of along, the external field in the rhombohedral phase. Although the implications of these results for our [001] and [110] electric field measurements are not yet clear, they do indicate that the field can greatly affect the PNR configuration, and therefore the structural inhomogeneity.[24,25]

C. Extension of T and/or O phase fields to lower x by E

In the ZFC phase diagram of PMN-xPT, the T phase extends only to $x=0.30$; and for $x<0.30$, a $C \rightarrow R$ sequence is found on cooling. For the [001] FC crystals, the T phase was extended to $x=0.25$, and could be induced by fields as small as $E=0.25$ kV/cm for $x=0.28$. However, for the [110] FC crystals, the region where the T phase was extended was entirely replaced by the O phase.

Following the phase diagrams in Fig. 2, it can be noted that the M_C and O phases are closely related to the presence of a stable T phase, whereas M_A and M_B are always connected to R. Thus, we can conclude that for compositions on the left side of the MPB ($x<0.30$), the polarization rotation pathway is $R \rightarrow M_A \rightarrow T$ for $E\|[001]$ and $R \rightarrow M_B \rightarrow O$ for $E\|[100]$ with increasing E beginning from the ZFC condition; and that for compositions inside the MPB ($0.30<x \leqslant 0.35$), the path is $M_C \rightarrow T$ for $E\|[001]$, but $M_C \rightarrow O$ for $E\|[110]$. A special case occurs for PMN-0.30PT: the rotational pathway is $R \rightarrow M_A \rightarrow M_C \rightarrow T$ with increasing E from the ZFC state, due to a monoclinic M_A to M_C transition.

In the PMN-xPT crystalline solution, the substitution of the octahedron $[TiO_4]^{4-}$ for the more complex $[Mg_{1/2}Nb_{2/3}O_4]^{4-}$, between the relaxor PMN and ferroelectric PT, results in a MPB separating ferroelectric R and T phases. In the T-phase field, the tetragonal splitting is known to be weakened with decreasing x.[14,26] For $x=0.30$ in the ZFC condition, the T phase is only observed over a narrow range of temperatures; furthermore, relaxor ferroelectric behavior has been reported in ZFC crystals for $x \leqslant 0.30$. Thus, PMN-0.30PT can be considered as a special composition in the phase diagram, where a gradual transition between microdomains of the T phase and a macroscopic T phase begins to occur. We note that microdomains have been observed by electron microscopy for $0<x<0.30$.[27] Since these microdomains are much smaller than the coherence length of x rays, the structure appears cubic below T_M in the ZFC state. However, in the FC state, the microdomains align along the direction that E is applied. Thus, an extended macroscopic T phase is observed to be sandwiched between the C and M_A phases on cooling for $0.25 \leqslant x < 0.30$, whose c/a ratio can be significantly altered by E. However, more thought is required

to understand the presence of microdomains and intermediate orthorhombic and monoclinic phases.

D. Fragile phase stability of PMN-*x*PT

Consider for example PMN-0.28PT. *T* and *O* phases were found in the same temperature range for $E\|[001]$ and $E\|[110]$, respectively, under fields as small as $E=0.25$ kV/cm. However, comparison of the lattice parameters of the *T* and *O* phases (at the same temperature) reveals an interesting feature: $a_T \approx b_O \approx 4.020$ Å and $a_O/\sqrt{2}+c_O/\sqrt{2}=a_T+c_T\approx 8.049$ Å (365 K). Similar observations were made at other temperatures and for $x=0.30$,[17] 0.35.[22] Since the *O* phase is the limiting case of the M_C one, we observed an equally important relationship between the lattice parameters of the *T* and M_C phases for $x=0.30$,[17] 0.32,[16] 0.35:[22] $b_M=a_T$, and $a_M+c_M=a_T+c_T$ where a_M, b_M, and c_M are the lattice parameters of the M_C unit cell. These observations demonstrate the existence of an important crystallographic relationship or transformation between the *T*, *O*, and M_C phases—they are not independent of each other.

Recently, a theory of an adaptive ferroelectric phase[28–30] has been developed to predict the microdomain-averaged crystal lattice parameters of a structurally inhomogeneous state, consisting of tetragonal microdomains. This theory predicts crystallographic relationships between *T* and M_C phases of

$$a_M + c_M = a_T + c_T, \tag{1a}$$

$$b_M = a_T, \tag{1b}$$

which have been experimental verified for PMN-*x*PT and PZN-*x*PT. Recently, Wang *et al.*[31] have extended this analysis, obtaining a relationship between the monoclinic angle (β) and the tetragonal and monoclinic lattice parameters, given as

$$\beta = 90^\circ + 2A\omega(1-\omega)\left(\tan^{-1}\frac{c_T}{a_T} - 45^\circ\right), \tag{1c}$$

where $\omega=(c_M-b_M)/(a_M+c_M-2b_M)$, $a_T=b_M$, $c_T=a_M+c_M-b_M$, and the constant $A\approx 1$. Furthermore, we note that the *O* phase is a limiting case of M_C, where $\omega=\frac{1}{2}$.

The predictions of (1) are identical to the experimentally observed relationship between the *T*, *O*, and M_C lattice parameters that we noted above. These observations provide quantitative evidence that the M_C and *O* phases are adaptive phases consisting of tetragonal microdomains. Application of $E\|[110]$ fixes the [110] orientation, where the [100] and [001] variants of tetragonal microdomains are of equal volume fraction: thus, the stable phase appears to be a single-domain orthorhombic one; whereas for $E\|[001]$, the volume fraction of the tetragonal microdomains variants is variable and not equivalent: thus, the stable phase appears to be polydomain M_C.

In summary, the results of this investigation demonstrate that the phase stability is "fragile:" the phase diagrams can be altered by application of modest electric fields along different crystallographic axes. However, comparison of the lattice parameters of the different phase fields shows that the fragility may only be a perception—the lattice parameters of the *O*, M_C, and *T* phase are interrelated. Analysis of the lattice parameters suggests that in fact the *O* and M_C phases consist of tetragonal microdomains that are geometrically aligned with respect to each other, in a manner to achieve stress accommodation. In this case, the *O* and M_C phases may appear to be uniform on a length equivalent to or larger than the coherence length of x rays, but in fact consists of structurally inhomogeneous phases of tetragonal microdomains on a local scale.

ACKNOWLEDGMENTS

We would like to gratefully acknowledge financial support from the Office of Naval Research under Grants No. N000140210340, No. N000140210126, and MURI No. N0000140110761; and from the U.S. Department of Energy under Contract No. DE-AC02-98CH10886. We would like to thank H. C. Materias for providing the single crystals used in this study.

APPENDIX

Although the existence of M_A and M_B phases in PMN-*x*PT has long been predicted by Vanderbilt and Cohen using a thermodynamic theory,[19] it is not easy to distinguish these two phases in experiments. For the M_A phase, $P_x=P_y<P_z$; whereas for M_B phase, $P_x=P_y>P_z$. However, in structural measurements, comparing P_x, P_y, and P_z is not always straightforward. Here we discuss a robust but easy-to-use criterion that can be applied to structural measurements.

A schematic for the M_A and M_B phases is shown in Fig. 1(b). Here we show the plane defined by the [110] and [001] vectors. In both monoclinic phases, [110] (a_m) is tilted up toward [001] (c_m), and the lengths of a_m and c_m also deviate from those in the cubic phase (in the cubic phase, $a_m=\sqrt{2}a=\sqrt{2}c$). Therefore, the ratio $a_m/\sqrt{2}c_m$ and the monoclinic angle β between a_m and c_m are the only two parameters necessary to define a M_A or M_B phase.

For a monoclinic phase with a fixed monoclinic angle β, the polarization components (P_x,P_y,P_z) are exclusively determined by the ratio $a_m/\sqrt{2}c_m$. The phase is M_A if the polarization falls closer to the [001] direction (*T*), M_B if the polarization falls closer to the [110] direction (*O*). The severing point between M_A and M_B is therefore the phase where $P_x=P_y=P_z$, which is a rhombohedral phase (*R*).

This provides a definitive way to distinguish M_A and M_B based on β and $a_m/\sqrt{2}c_m$. When we have a M_A- or M_B-type structure, we should compare its $a_m/\sqrt{2}c_m$ ratio to that of the rhombohedral phase which has the same angle β between its [001] and [110] vectors. For example, for a rhombohedral phase with rhombohedral angle α^* (angle between [001] and [100]), the ratio $a_m^*/\sqrt{2}c_m^*$ (here a_m^* denotes the length along the [110] direction) is $\sqrt{2}\cos(\alpha^*/2)$, while α^* also has to satisfy $\cos(\beta)=[1-2\sin^2(\alpha^*/2)]/\cos(\alpha^*/2)$ for the angle between [001] and [110] to be β. If $a_m/\sqrt{2}c_m$ from our measurements is greater than $\sqrt{2}\cos(\alpha^*/2)$, we have a M_B phase, otherwise we have a M_A phase.

Since for most cases in lead perovskite relaxors, α and β are very close to 90°, $\sqrt{2}\cos(\alpha^*/2)$ is close to 1. In practice, people usually can compare $a_m/\sqrt{2}c_m$ to 1 to determine whether the structure is a M_A or M_B phase.[15,17,26] However, when $a_m/\sqrt{2}c_m$ is close to 1, the method described here should be used.

[1] S.-E. Park and T. R. Shrout, J. Appl. Phys. **82**, 1804 (1997).
[2] H. S. Luo, G. S. Xu, H. Q. Xu, P. C. Wang, and Z. W. Yin, Jpn. J. Appl. Phys., Part 1 **39**, 5581 (2000).
[3] W. R. Cook and H. Jaffe, *Piezoelectric Ceramics* (Academic, London, 1971), p. 136.
[4] S. F. Liu, S-E. Park, T. R. Shrout, and L. E. Cross, J. Appl. Phys. **85**, 2810 (1999).
[5] B. Noheda, D. E. Cox, G. Shirane, J. A. Gonzalo, L. E. Cross, and S.-E. Park, Appl. Phys. Lett. **74**, 2059 (1999).
[6] B. Noheda, J. A. Gonzalo, L. E. Cross, R. Guo, S.-E. Park, D. E. Cox, and G. Shirane, Phys. Rev. B **61**, 8687 (2000).
[7] B. Noheda, D. E. Cox, G. Shirane, R. Guo, B. Jones, and L. E. Cross, Phys. Rev. B **63**, 014103 (2000).
[8] B. Noheda, D. E. Cox, G. Shirane, S. E. Park, L. E. Cross, and Z. Zhong, Phys. Rev. Lett. **86**, 3891 (2001).
[9] D. La-Orauttapong, B. Noheda, Z. G. Ye, P. M. Gehring, J. Toulouse, D. E. Cox, and G. Shirane, Phys. Rev. B **65**, 144101 (2002).
[10] B. Noheda, Z. Zhong, D. E. Cox, G. Shirane, S. E. Park, and P. Rehrig, Phys. Rev. B **65**, 224101 (2002).
[11] K. Ohwada, K. Hirota, P. Rehrig, Y. Fujii, and G. Shirane, Phys. Rev. B **67**, 094111 (2003).
[12] J. M. Kiat, Y. Uesu, B. Dkhil, M. Matsuda, C. Malibert, and G. Calvarin, Phys. Rev. B **65**, 064106 (2002).
[13] Z. G. Ye, B. Noheda, M. Dong, D. Cox, and G. Shirane, Phys. Rev. B **64**, 184114 (2001).
[14] B. Noheda, D. E. Cox, G. Shirane, J. Gao, and Z. G. Ye, Phys. Rev. B **66**, 054104 (2002).
[15] F. Bai, N. Wang, J. Li, D. Viehland, P. Gehring, G. Xu, and G. Shirane, J. Appl. Phys. **96**, 1620 (2004).
[16] Hu Cao, Feiming Bai, Jiefang Li, D. Viehland, Guangyong Xu, H. Hiraka, and G. Shirane, J. Appl. Phys. **97**, 094101 (2004).
[17] Hu Cao, Feiming Bai, Naigang Wang, Jiefang Li, D. Viehland, Gangyong Xu, and Gen Shirane, Phys. Rev. B **72**, 064104 (2005).
[18] H. Fu and R. E. Cohen, Nature (London) **403**, 281 (2000).
[19] D. Vanderbilt and M. H. Cohen, Phys. Rev. B **63**, 094108 (2001).
[20] F. Jona and G. Shirane, *Ferroelectric Crystals* (Pergamon Press, New York, 1962).
[21] Y. Lu, D.-Y. Jeong, Z.-Y. Cheng, Q. M. Zhang, H. Luo, Z. Yin, and D. Viehland, Appl. Phys. Lett. **78**, 3109 (2001).
[22] Hu Cao, Jiefang Li, and D. Viehland, Appl. Phys. Lett. **88**, 072915 (2006).
[23] Hu Cao, Jiefang Li, and D. Viehland (unpublished).
[24] Guangyong Xu, P. M. Gehring, and G. Shirane, Phys. Rev. B **72**, 214106 (2005).
[25] Guangyong Xu, Z. Zhong, Y. Bing, Z.-G. Ye, and G. Shirane, Nat. Mater. **5**, 134 (2006).
[26] A. K. Singh and D. Pandey, Phys. Rev. B **67**, 064102 (2003).
[27] D. Viehland, J. Appl. Phys. **88**, 4794 (2000).
[28] Z. Xu, M. Kim, J. Li, and D. Viehland, Philos. Mag. A **79**, 305 (1996).
[29] Y. M. Jin, Y. U. Wang, A. G. Khachaturyan, J. F. Li, and D. Viehland, J. Appl. Phys. **94**, 1 (2003).
[30] Y. M. Jin, Y. U. Wang, A. G. Khachaturyan, J. F. Li, and D. Viehland, Phys. Rev. Lett. **91**, 197601 (2003).
[31] Yu Wang, Phys. Rev. B **73**, 014113 (2006).